Interconnect Energy Dissipation in High-Speed ULSI Circuits

Payam Heydari
Department of Electrical and Computer Engineering
University of California
Irvine, CA 92697

Massoud Pedram
Department of Electrical Engineering-Systems
University of Southern California
Los Angeles, CA 90089

Abstract - *This work presents accurate closed-form expressions for the interconnect energy dissipation in high-speed ULSI circuits. Unlike previous works, the energy is calculated using an approximated expression for the driving-point impedance of lossy coupled transmission lines which itself is derived by solving Telegrapher's equations. The effect of electromagnetic (inductive and capacitive) couplings on the energy dissipation is accounted for in the derivations. We synthesize a new stable circuit that is capable of modeling the transmission line for a broad range of frequencies. Experimental results show that the energy calculated using this equivalent circuit is almost equal to the one calculated by solving the more complicated transmission line equations directly.*

1. Introduction

The International Technology Roadmap for Semiconductors (ITRS) predicts that by 2010 over one billion transistors will be integrated into a single monolithic die [1]. The wiring system of this one-billion transistor die will deliver signal and power to each transistor on the chip, provide low-skew and low-jitter clock to latches, flip-flops and dynamic circuits, and also distribute data and control signals throughout the chip [2]. Providing the required global connectivity throughout the whole chip demands long on-chip wires. These global wires should deliver high frequency signals (presently at around 1-2GHz) to various circuits. This implies that the global wires exhibit transmission line effects including electromagnetic coupling. On the other hand, as technology sizes continue to decrease, many new effects are being observed due to the use of nanometer technologies. Some significant deep sub-quarter-micron effects are caused by increasing cross-coupling capacitance and coupling inductance. So far, the well-known $(1/2)CV^2$ model has been used as an interconnect energy model, where C includes the capacitance of the interconnect and the capacitances of the driven circuits, and V is the voltage swing. This model, however, fails to predict the interconnect energy dissipation in the current range of clock frequencies, where the signal transients do not usually settle to a steady state value due to the small clock periods. Moreover, this model does not consider coupling noise as well as other transmission line properties. As we will see in this paper, these effects must be accounted for in the energy calculations that will otherwise lead to erroneous results. In paper [3], an analytical interconnect energy model with consideration of event coupling has been proposed. Although this work considers the crosstalk effect on the interconnect energy dissipation, it uses the distributed ladder RLC circuits to model the lossy transmission line effects. In paper [4], authors showed that using distributed RLC circuits do not capture all behaviors of lossy transmission lines that can be captured otherwise using the transmission line equations.

In this paper, accurate expressions for the energy dissipation of coupled interconnects are obtained while addressing two important problems simultaneously. The first problem is to analyze the transmission line effects on the energy dissipations. The second problem is to consider the effect of electromagnetic coupling on the interconnect energy dissipation.

Section 2 gives a comprehensive analysis of energy dissipation in RLC circuits. This analysis provides helpful observations regarding the energy calculations that are extensively used in section 3. In section 3, a new RLC circuit configuration is synthesized whose input impedance can accurately estimate the driving-point impedance of coupled lossy transmission line. Using this circuit we derive the total energy dissipation of coupled lossy transmission lines. Simulations and experimental results provided throughout this section confirms the accuracy of our model. Finally, section 4 presents the conclusions of our paper.

2. Energy dissipation of passive RLC circuits

One common way of studying the parasitic effects of an on-chip interconnect on the performance of a VLSI circuit is to model it by a large number of cascaded ladder RLC circuits. Therefore a relevant starting point for studying the energy dissipation of on-chip interconnects is to investigate the energy dissipation of a passive RLC circuit, demonstrated in Fig. 1, that is excited by a unit step voltage. Depending on the relative values of the circuit elements, this circuit exhibits either of the two possible transient responses as also depicted in Fig. 1.

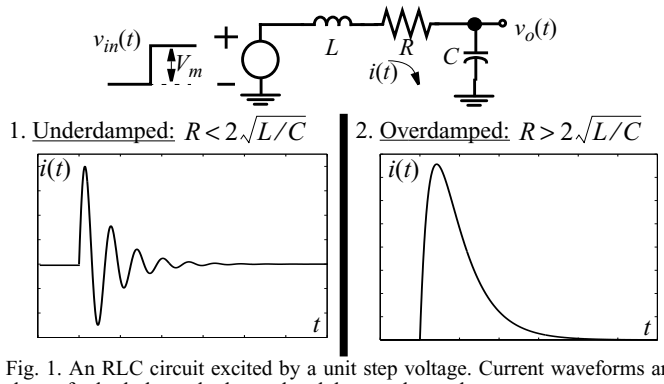

Fig. 1. An RLC circuit excited by a unit step voltage. Current waveforms are shown for both the underdamped and the overdamped cases.

The total energy delivered by the input source to the passive circuit is as follows:

$$E_{tot} = \int_{-\infty}^{\infty} v_{in}(t)i(t)dt \tag{1}$$

In the next two sub-sections we obtain the total as well as the dissipated energy for both underdamped and overdamped RLC circuits.

2.a. Energy dissipation of an underdamped RLC circuit

In the underdamped case, the voltage and current transient waveforms oscillate toward their steady-state values. This transient behavior occurs when $R < 2\sqrt{L/C}$. In terms of energy, the stored energy in the capacitor and/or in the inductor is being transferred back and forth between reactive elements. If the circuit is lossless ($R = 0$), this energy transfer will be performed endlessly. However with a resistor present in the circuit, a portion of the energy is dissipated in the resistor. To obtain the energy dissipated by the circuit, we first obtain the total energy generated by the input source.

$$E_{u,\,tot} = \int_{0}^{\infty} V_m i_u(t)dt \tag{2}$$

where $i_u(t)$ is the current flowing through the underdamped circuit. This current is easily obtained by solving the characteristic differential equation of the RLC circuit.

$$i_u(t) = \left(\frac{V_m}{L}\right)\frac{1}{\omega_d}e^{-\alpha t}\sin\omega_d t \tag{3}$$

where α, the damping constant, is $\alpha = R/2L$, ω_n, the resonant frequency, is $\omega_n^2 = 1/LC$, and ω_d, the oscillation frequency, is equal to $\omega_d = \sqrt{\omega_n^2 - \alpha^2}$. Replacing the $i_n(t)$ in Eq. (2) with its equivalent expression given in Eq. (3) and computing the resulting integral leads to the following equation:

$$E_{u,\,tot} = \int_0^\infty V_m \left(\frac{V_m}{L}\right)\frac{1}{\omega_d} e^{-\alpha t} \sin\omega_d t \; dt = \frac{V_m^2}{L\omega_n^2} = CV_m^2 \qquad (4)$$

For the passive RLC circuit driven by a unit step function, the magnetic energy across the inductor is transferred to the electric energy across the capacitor in the steady-state. Therefore, the total stored energy in reactive elements is $(1/2)CV_m^2$. Consequently, the energy dissipated in a passive underdamped RLC circuit is as follows:

$$E_{u,\,dissipated} = E_{u,\,tot} - \frac{1}{2}CV_m^2 = \frac{1}{2}CV_m^2 \qquad (5)$$

From Eq. (5) it is concluded that the energy dissipated in any passive underdamped RLC circuit that is driven by a unit step function is simply $(1/2)CV_m^2$.

Now let us assume that the input source to the RLC circuit is a periodic rectangular waveform, which is almost the case in digital integrated circuits. The total energy delivered by the input source during the low-to-high transition of the input source is as follows:

$$E_{u,\,tot}^{RLC} = CV_m^2\left[1 - \left(\frac{\omega_n}{\omega_d}\right)e^{-\frac{\alpha T}{2}}\sin\left(\frac{\omega_d T}{2} + \Phi\right)\right] \qquad (6)$$

Fig. 2 shows the energy variation as a function of the fundamental period, *T*, for an underdamped RLC circuit excited by a periodic rectangular voltage signal. Please note that for small periods, the $(1/2)CV^2$ energy model gives rise to a wrong value.

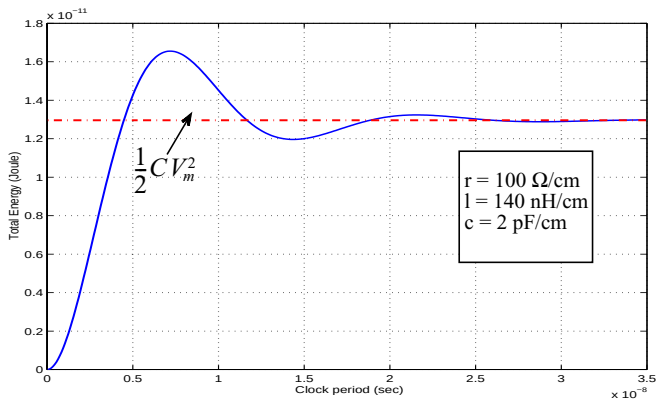

Fig. 2. The total delivered energy vs. the fundamental periods of oscillations for an underdamped RLC circuit

The dissipated energy in the low-high transition of the input source is:

$$E_{u,\,dissipated}^{L\to H} = \int_0^{T/2} R i_u^2(t)\,dt$$

$$E_{u,\,dissipated}^{L\to H} = \frac{1}{2}CV_m^2\left[1 - \left(\frac{\omega_n}{\omega_d}\right)^2 e^{-\alpha T}(1 - \cos(\omega_d T - \Phi)\cos(\Phi))\right] \qquad (7)$$

In equations (6) and (7), $\Phi = \mathrm{atan}(\omega_d/\alpha)$. As *T*, the fundamental period of the input waveform, becomes larger, the second term inside the bracket becomes smaller, and in the limit, the energy expression becomes identical to Eq. (5).

❐

2.b. Energy dissipation of an overdamped RLC circuit

In the overdamped case, the resistor is sufficiently large (i.e., $R > 2\sqrt{L/C}$) such that it eliminates the resonances from current and voltage waveforms. The total energy delivered by the input source is the same as Eq. (1), which is rewritten here for convenience.

$$E_{o,\,tot} = \int_0^\infty V_m i_o(t)\,dt \qquad (8)$$

where $i_o(t)$ is the current flowing through the overdamped circuit. This current is easily obtained by solving the characteristic differential equation of the RLC circuit.

$$i_o(t) = \left(\frac{V_m}{2L}\right)\frac{1}{\alpha_d}e^{-\alpha t}(e^{\alpha_d t} - e^{-\alpha_d t}) = \left(\frac{V_m}{L}\right)\frac{1}{\alpha_d}e^{-\alpha t}\sinh\alpha_d t \qquad (9)$$

where $\alpha_d = \sqrt{\alpha^2 - \omega_n^2}$. The total delivered energy is:

$$E_{o,\,tot} = \int_0^\infty V_m\left(\frac{V_m}{2L}\right)\frac{1}{\alpha_d}e^{-\alpha t}(e^{\alpha_d t} - e^{-\alpha_d t})\,dt = \frac{2V_m^2}{2L\omega_n^2} = CV_m^2 \qquad (10)$$

Similar to the underdamped case, consider a periodic rectangular waveform at the input. The total energy delivered by the input source is:

$$E_{o,\,tot}^{RLC} = CV_m^2\left[1 - \left(\frac{\omega_n}{\alpha_d}\right)e^{-\frac{\alpha T}{2}}\sinh\left(\frac{\alpha_d T}{2} + \Psi\right)\right] \qquad (11)$$

Fig. 3 shows the energy variation in terms of the variation in the fundamental period. The error caused by using the $(1/2)CV^2$ model in the overdamped case is smaller than that in the underdamped case. However, in practice, the underdamped response is occurred more frequently.

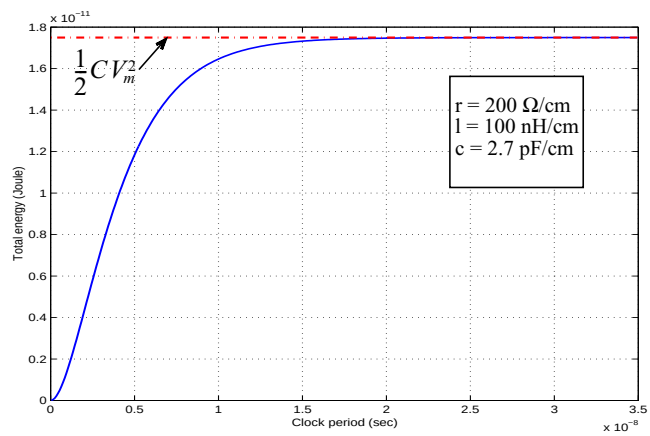

Fig. 3. The total delivered energy vs. the fundamental periods of oscillations for an overdamped RLC circuit

The energy dissipated in the low-high transition of the input source will be as follows:

$$E_{o,\,dissipated}^{L\to H} = \frac{1}{2}CV_m^2\left[1 + \left(\frac{\omega_n}{\alpha_d}\right)^2 e^{-\alpha T}(1 - \cosh(\alpha_d T + \Psi)\cosh(\Psi))\right] \qquad (12)$$

In equations (11) and (12), $\Psi = \mathrm{atanh}(\alpha_d/\alpha)$. As *T* becomes larger the energy expression approaches $(1/2)CV_m^2$.

❐

2.c. Frequency-domain analysis

From the above analysis some valuable conclusions are drawn. First of all, the energy dissipation of a passive RLC circuit excited by a *unit step* input is $(1/2)CV_m^2$ irrespective of the circuit conditions (i.e., overdamped or underdamped). From another perspective, the capacitor charges up to the input step voltage, V_m, and in the steady-state is modeled as an open circuit. Therefore, the total stored energy appears as electric field energy across the capacitor ($(1/2)CV_m^2$). One important concern is to find out a circuit interpretation of the total energy generated by the input source. To address this concern, consider the driving-point admittance of RLC circuit of Fig. 1.

$$Y_{in}(s) = \frac{s/L}{s^2 + 2\alpha s + \omega_n^2} \qquad (13)$$

$Y_{in}(s \to 0$ represents the equivalent DC driving-point admittance of an RLC circuit in the steady-state condition. This is an important notion that will be utilized later on during the simplification of the driving-point admittance as well as the derivation of the energy dissipation of a coupled transmission line. Direct calculations reveal that $Y_{in}(s \to 0) = Cs$. Hence the steady-state current is an impulse function, and the total delivered energy by the source as follows:

$$E_{tot} = \int_0^{\infty} V_m i(t)\,dt = \int_0^{\infty} V_m^2 C\delta(t)\,dt = CV_m^2 \tag{14}$$

As a generalization, consider a ladder circuit consisting of N RLC circuits with a unit step input as shown in Fig. 4.a. The equivalent circuit for the energy analysis of each RLC subsection contains only the capacitor of that RLC subsection. The equivalent circuit is depicted in Fig. 4.b. The total energy delivered by the source is:

$$E_{tot} = \int_0^{\infty} V_m i(t)\,dt = \left(\sum_{k=1}^{N} C_k\right) V_m^2 \tag{15}$$

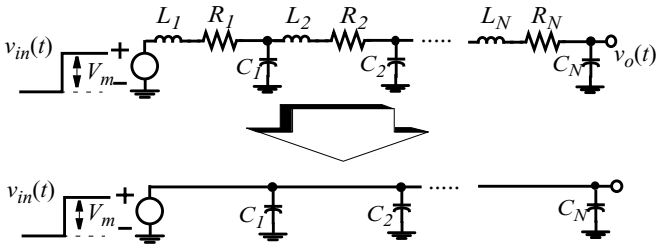

Fig. 4. A ladder of cascaded RLC circuits. (a) the circuit schematic. (b) the equivalent circuit for the energy analysis

The above discussion will be widely used in the following sections.

3. Energy dissipation of lossy transmission lines

Thus far the main attention has been focused on the energy analysis of single passive RLC circuits. There are, however, two major questions that also need to be addressed. In present-day digital and mixed-signal integrated circuits, the global on-chip interconnects must provide the required connectivity and performance for clock rates of 1.0-2.0GHz, which is in a microwave frequency range. This certainly demands a knowledge of electromagnetic-field theory to analyze the on-chip wiring effects. A related question that arises is whether the transmission line effects of on-chip interconnects can have any affect on the energy dissipation. On the other hand, high wiring density and high operating frequencies result in high capacitive and inductive coupling. Consequently, the second question is whether the electromagnetic coupling has any impact on the energy dissipation. This section indeed addresses these questions.

The critical global interconnections, such as clock lines, control lines, and data buses (which can be 32-128 bits wide) between processor and on-chip cache reach more than 100K connections. The propagation delay of signals traveling through these global wires is comparable to the time of flight. In other words, the line length is comparable to the propagated signal wavelength, λ, which is on the order of 0.7-2.2cm. This implies that transmission-line properties have to be taken into account. It was shown in [4] that any two uniform parallel conductors, the signal and the return paths, that are used to transmit electromagnetic energy can be considered transmission lines. The return path can be a ground plane, a ground conductor, or a mesh of ground lines on many layers. Solutions to Maxwell's equations for the electric and magnetic fields around conductors are current and voltage waves. The solution is completely determined in terms of the *characteristic impedance*, Z_o, and the *propagation constant*, γ. Consider a single transmission line as shown in Fig. 5. The voltage and current in the frequency domain at any point x along the line is expressed as a combination of incident and reflected waves.

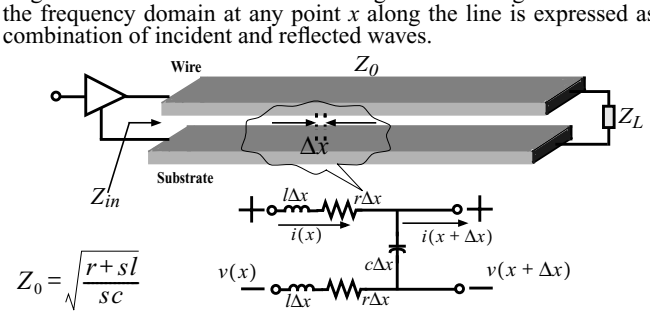

Fig. 5. The schematic of a lossy transmission line along with the circuit representation of a differential length Δx

$$V(x,s) = V_i e^{-\gamma x} + V_r e^{\gamma x} \tag{16}$$

$$I(x,s) = I_i e^{-\gamma x} - I_r e^{\gamma x} \tag{17}$$

where $\gamma = \sqrt{(r+sl)cs}$. The load termination determines how much of the wave is reflected upon arrival at the wire end. The *reflection coefficient*, Γ_L , determines the amount of the incident wave that reflects back to the line as a result of impedance mismatch between the line and the load.

$$\Gamma_L = \frac{Z_L - Z_0}{Z_L + Z_0} \tag{18}$$

The concept of the reflection coefficient is generalized to define the reflected and incident quantities at any arbitrary point along the line.

$$\Gamma(x) = \frac{V_r(0)e^{\gamma x}}{V_i(0)e^{-\gamma x}} = \Gamma_L e^{2\gamma x} \tag{19}$$

The driving point impedance, Z_{in}, is the ratio of the voltage and current waves at the input source end.

$$Z_{in}\big|_{x=-h} = \frac{V_i e^{\gamma h} + V_r e^{-\gamma h}}{I_i e^{\gamma h} - I_r e^{-\gamma h}} = Z_0\left(\frac{1+\Gamma_L e^{-2\gamma h}}{1-\Gamma_L e^{-2\gamma h}}\right) = Z_0\,\frac{Z_L + Z_0\tanh(\gamma h)}{Z_0 + Z_L\tanh(\gamma h)} \tag{20}$$

where h is the line length. In the above equation, the load impedance, Z_L, is normally a capacitive load in ULSI circuits, since the interconnect normally drives a CMOS circuit whose input impedance is purely capacitive.

To account for the electromagnetic coupling effects on the interconnect energy dissipation, the total line inductance and capacitance per unit length are modified accordingly. The effect of capacitive coupling is predicted by considering the switching transients of the immediate neighboring wires. The effect of nonadjacent lines are ignored because the capacitive coupling has a near-field effect, and the adjacent aggressive lines behave as shield lines for non-adjacent wires. On the contrary, the inductive coupling has a far-field effect. The non-adjacent lines have a considerable amount of inductive couplings on the victim line. This makes the analysis of inductive coupling particularly difficult. In addition, the current return paths cannot be easily configured [4] in the circuit. This causes the problem of inductive coupling to become even more complicated.

The effect of capacitive coupling is taken into account by using the Miller theorem as also shown in Fig. 6.

The Miller capacitance per unit length seen across the input port of the transmission line 1 as a result of switching in line 2 is:

$$c_{c,M} = c_c\left(1 - \frac{V_2(-h,s)}{V_1(-h,s)}\right) \tag{21}$$

The voltage waves V_2 and V_1 are obtained by combining their incident and reflected wave components at their corresponding input ports, similar to Eq. (16). To verify the accuracy of Eq. (21), the two transmission lines in Fig. 6 are simulated using star-HSPICE.

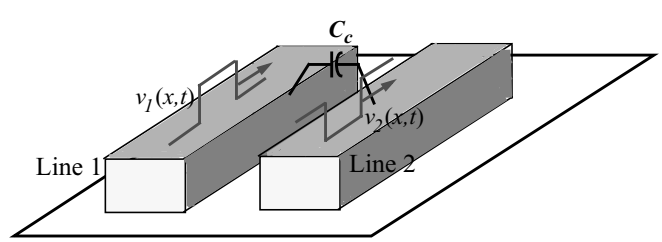

Fig. 6. Two capacitively coupled transmission lines. The traveling voltage waves are 180° out of phase.

Input sources are 180° out of phase as depicted in Fig. 6. Fig. 7.a shows current and voltage waveforms of line 1. We then decouple line 1 from line 2 by replacing cross-coupling capacitance c_c with its Miller capacitance $c_{c,M}$ in line 1, and then simulate this new circuit with HSPICE again. The voltage and current waveforms are depicted

in Fig. 7.b. Comparing voltage and current waveforms in Fig. 7.a with those in Fig. 7.b verifies the accuracy of Eq. (21).

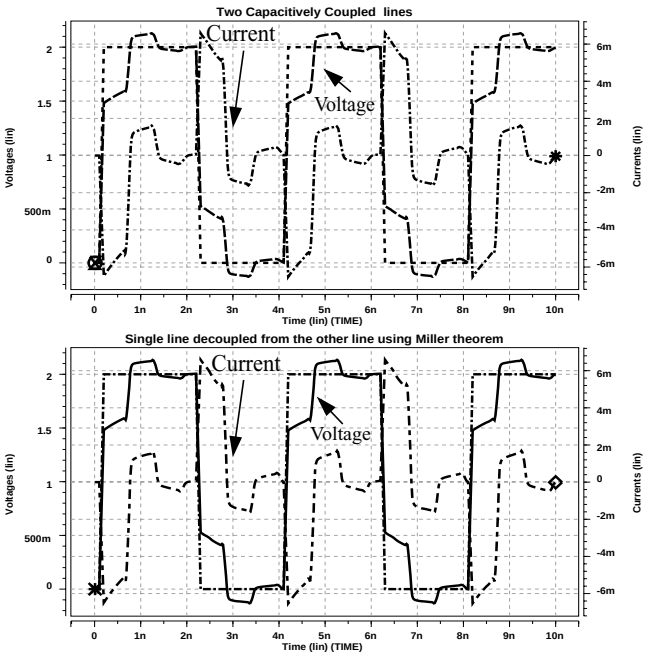

Fig. 7. The source voltage as well as driving-point current and voltage waveforms in a lossy coupled transmission line. (a) results obtained using HSPICE simulation on the coupled line. (b) results obtained using HSPICE on the decoupled line after applying Miller theorem

The inductive couplings between transmission lines are accounted for by an algebraic summation of each line's self inductance and all mutual inductances between that line and other lines considering also the current direction flowing through the lines. For example in a set of N coupled transmission lines, the total per unit length inductance of the *j*-th line that is magnetically coupled to other lines is:

$$l_{int,tot_j} = l_{int_j} + \sum_{i \neq j} (\pm M_{ij})$$

After characterizing the capacitive and inductive couplings, the next step is to obtain a relevant rational expression for the driving-point impedance of a coupled transmission line. According to Eq. (20), the input impedance of a transmission line is a nonlinear function of frequency. Direct substitution of this nonlinear expression into the energy equation does not yield a closed-form expression for the energy dissipation of the lossy transmission line. Still it is possible to simplify Eq. (20), using some observations, and obtain an accurate expression for the energy dissipation. According to section 2.c, if the abrupt transitions of the input waveform are sufficiently far away in time so as to allow the circuit to come very close to its steady-state response, then the total energy delivered by the source is evaluated using the driving point impedance at low frequencies. This observation is utilized here to simplify Eq. (20). First we evaluate *tanh*(·) at low frequencies:

$$\tanh(\gamma h) = \frac{\sinh(\gamma h)}{\cosh(\gamma h)} \rightarrow \frac{2\gamma h}{2+\gamma^2 h^2} \quad , \textit{for small values of } |s| \qquad (22)$$

This leads to the following relationship:

$$Z_{in}\big|_{x=-h} = \frac{1}{C_L s}\left[\frac{2+\gamma^2 h^2 + \left(2\gamma^2 h^2 \dfrac{C_L}{C_{int,tot}}\right)}{2+\gamma^2 h^2 \quad + \left(2\dfrac{C_{int,tot}}{C_L}\right)}\right] \qquad (23)$$

where $C_{int,tot}$ is the interconnect capacitance including the Miller capacitance and the interconnect-substrate capacitance. To find out how accurately Eq. (23) can predict the actual driving-point impedance of a lossy line, we utilize the per unit length parameters of the top-level metal layer in 0.11μ technology that are directly calculated from interconnect parameters provided by ITRS [1]. A comparison is made between magnitude response of the driving-point impedance given by Eq. (20) and the magnitude response of the expression in Eq. (23) for four different lengths. Fig. 8 shows such a comparison in a logarithmic scale. Obviously, the approximation is accurate in a broad range of frequencies. For longer lengths of the line the discrepancy begins to appear in lower frequencies.

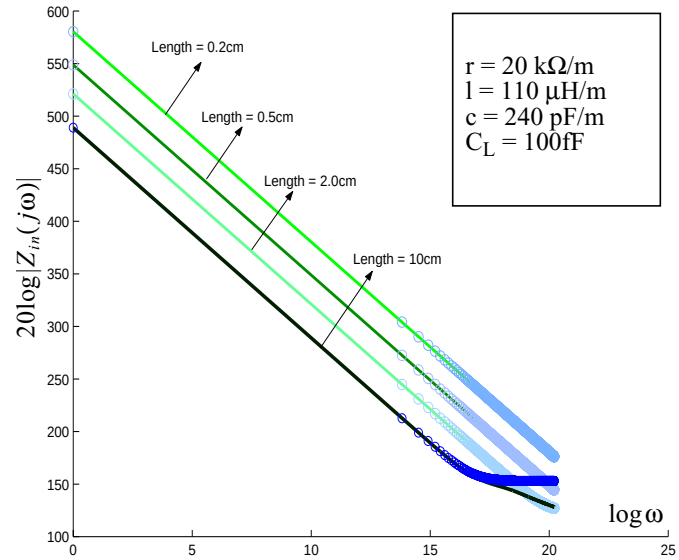

Fig. 8. A comparison between the magnitude response of line's actual driving-point impedance (Eq. (20)) and that of line's approximated rational impedance function (Eq. (23)) for four different line lengths

It would be instructive if one could propose a stable circuit realization whose impedance is expressed by Eq. (23). For a lossy transmission line whose driving-point impedance near the DC frequency is expressed by Eq. (23), a stable RLC-π equivalent circuit realization can be synthesized as demonstrated in Fig. 9. $L_{int,tot}$ is the total inductance of the lossy line including the self and mutual inductances, and R_{int} is the line resistance. C_1, C_2, and C_3 are related to actual capacitances of the line and the load through the following relationships:

$$C_3 = \sqrt{\frac{(C_{int,tot}+C_L)^2 + C_L^2}{2}}, C_2 = \frac{C_{int,tot}}{2} + C_L - C_3 \;,\; C_1 = C_{int,tot} + C_L - C_3 \qquad (24)$$

The input impedance of the transmission line in Fig. 9 in the low-frequency range is:

$$Z_{in,xline}(s) = \left(\frac{1+2C_L/C_{int,tot}}{C_L s}\right)\left(\frac{s^2 + \dfrac{R_{int}}{L_{int,tot}}s + \dfrac{2}{L_{int,tot}C_{int,tot}(1+2C_L/C_{int,tot})}}{s^2 + \dfrac{R_{int}}{L_{int,tot}}s + \dfrac{2(1+C_{int,tot}/C_L)}{L_{int,tot}C_{int,tot}}}\right) \qquad (25)$$

The input impedance of the RLC-π circuit shown in Fig. 9 is:

$$Z_{in,RLC}(s) = \frac{1}{(C_1 + C_2 \circledS C_3)s}\left(\frac{s^2 + \dfrac{R_{int}}{L_{int,tot}}s + \dfrac{1}{L_{int,tot}(C_2+C_3)}}{s^2 + \dfrac{R_{int}}{L_{int,tot}}s + \dfrac{(C_1+C_3)/(C_2+C_3)}{L_{int,tot}(C_1 + C_2 \circledS C_3)}}\right) \qquad (26)$$

where $C_2 \circledS C_3$ represents the series combination of C_2 and C_3. Equating the *s* coefficients of the driving-point impedance $Z_{in,xline}(s)$ of the transmission line with those of the input impedance $Z_{in,RLC}(s)$ of the proposed RLC circuit verifies circuit equivalence.

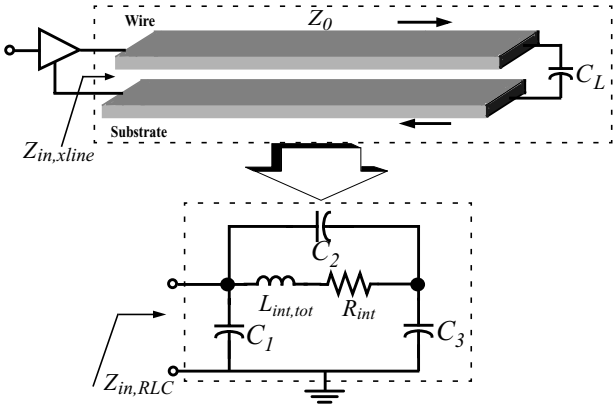

Fig. 9. A lossy transmission line and its equivalent RLC-π circuit representation

Fig. 10 shows the magnitude response of the driving-point admittance of a lossy transmission line which is electromagnetically coupled to a similar line. First, the circuit is simulated using star-HSPICE. Eq. (20) is then utilized and the magnitude response of the admittance function (which is the inverse of the impedance function) is calculated. As indicated in Fig. 10, the results obtained by HSPICE and by Eq. (20) are indistinguishable from each other. In the next step, Eq. (26) is utilized to calculate the magnitude response of the driving-point admittance for the equivalent RLC-π circuit. This circuit accurately represents the driving-point admittance of a lossy coupled transmission line in lower frequencies up to 1.6GHz. Consequently, the energy calculations using the RLC-π circuit yield the expressions that are exactly equal to those of the actual coupled lossy line.

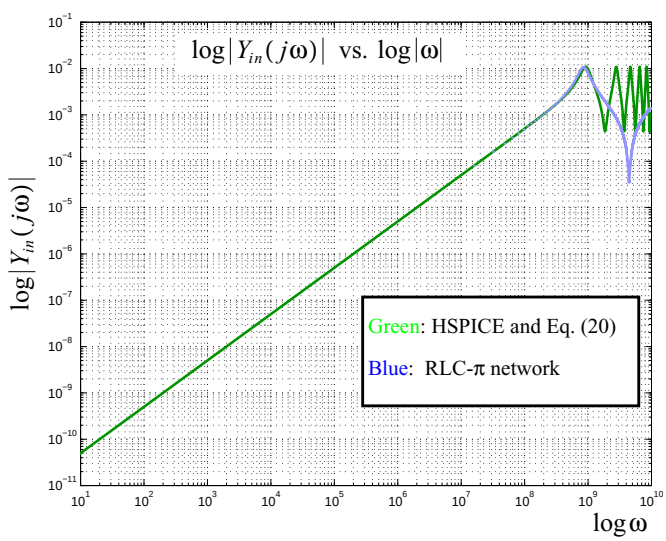

Fig. 10. The magnitude response of the driving point admittance of an electromagnetically coupled lossy transmission line obtained using HSPICE simulation, using the direct simulation of Eq. (20), and by replacing the line with its equivalent RLC-π circuit

The RLC-π equivalent circuit synthesized for a lossy coupled transmission line is used to compute the driving point impedance and interconnect energy calculation. The effect of the input source impedance on the total energy dissipation is readily taken into account by connecting the input terminal of the equivalent RLC-π to input source. The π structure of the RLC-π circuit makes the impedance calculations very simple. For instance, the diffusion capacitances of the driving CMOS circuits (C_d in Fig. 11) are placed directly in parallel with the capacitance, C_1 of the RLC-π circuitry and consequently no additional calculation is required.

To include the most complete scenario, consider a lossy transmission line that is coupled to other lines through magnetic as well as electric field couplings. Furthermore, suppose that this line is driven by a CMOS inverter. The load is another CMOS gate that is connected to the other port of this lossy transmission line. The coupling effects are treated the same way as we discussed earlier in this section. Fig. 6. shows the circuit that needs to be analyzed.

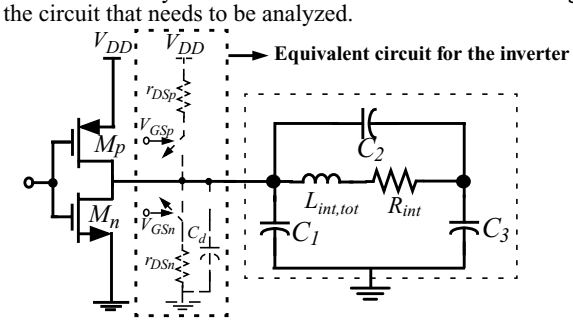

Fig. 11. The equivalent RLC-π circuit model of a lossy coupled transmission line driven by a CMOS inverter

Due to the changes in the operation regions of NMOS and PMOS transistors during low-to-high and high-to-low transitions of the driver's output, we must distinguish between low-to-high and high-to-low transitions. During the low-to-high transition the PMOS transistor is in the linear region and provides a conduction path from the supply to the load. During the high-to-low transition the NMOS transistor is in the linear region, and no additional energy is transferred out of the power-supply.

We calculate the energy transferred out of the power-supply during a low-to-high transition. This energy is the total dissipated energy per clock period of a CMOS gate that drives another CMOS circuit through a coupled lossy transmission line. The energy delivered by the power-supply through the gate in a low-to-high transition is specified by Eq. (1) where $v_{in}(t) = V_{DD}u(t)$) ($u(t)$ is the unit step function). The current is obtained using the driving point admittance of the circuit indicated by Fig. 11:

$$I_i(s) = \frac{V_{DD}}{s} Y_i(s)$$

where $Y_i(s)$ is the driving-point admittance seen from the power-supply to the source connection of the PMOS transistor in Fig. 11. $Y_i(s)$ is the parallel combination of $Y_{in,RLC}(s) = 1/Z_{in,RLC}(s)$ and the diffusion capacitance C_d of MOS devices. Once again we distinguish between the overdamped and the underdamped responses. We make use of the formulations given in section 2 to obtain the energy expression for each of these responses.

Underdamped response

Similar to the discussion in section 2.a, if $R_{int} < 2\sqrt{L_{int,tot}/(C_2+C_3)}$ then the current and voltage waveforms will oscillate until they reach their steady state value. Utilizing Eq. (3), the input current to the circuit is as follows:

$$i_{DD} = (C_d + C_{eq,\pi})V_{DD}\delta(t) + \frac{V_{DD}}{L_{int,tot}\omega_{d,\pi}}\left(\frac{C_3}{C_2+C_3}\right)^2 e^{-\alpha_\pi t}\sin\omega_{d,\pi}t \quad (27)$$

where $C_{eq,\pi} = C_1 + C_2 \circledS C_3$ is the equivalent capacitance of the RLC-π circuit, $\alpha_\pi = R_{int}/2L_{int}$, $\omega_{p,\pi}^2 = 1/(L_{int}(C_2+C_3))$, and $\omega_{d,\pi} = \sqrt{\omega_{p,\pi}^2 - \alpha_\pi^2}$. C_1, C_2, and C_3 are given by Eq. (24). The total energy delivered by the power-supply is:

$$E_{tu,tot}^{xline} = (C_d + C_1 + C_3)V_{DD}^2 - \left(\frac{C_3^2}{C_2+C_3}\right)V_{DD}^2\left(\frac{\omega_{p,\pi}}{\omega_{d,\pi}}\right)e^{-\frac{\alpha_\pi T}{2}}\sin\left(\frac{\omega_{d,\pi}T}{2} + \Phi_\pi\right) \quad (28)$$

Remember that $C_1 + C_3 = C_L + C_{int,tot}$. We observe that if a CMOS inverter driving a lossy coupled line undergoes an underdamped oscillatory response, and if $R_{int}/L_{int,tot} >> 4\pi f_{clock}$ (or if $1/(2\pi\sqrt{L_{int,tot}(C_2+C_3)}) >> 2f_{clock}$), then the energy expression becomes:

$$E_{tu,tot}^{xline} = (C_d + C_{int,tot} + C_L)V_{DD}^2 \quad (29)$$

Equations (28) and (29) give the actual and steady-state energy dissipation per clock period, respectively, when the circuit experiences an underdamped oscillatory transient response.

Overdamped response

We recall from section 2.b that if $R_{int} > 2\sqrt{L_{int,tot}/(C_2+C_3)}$, then we have overdamped response. Utilizing Eq. (9), the input current to the circuit is as follows:

$$i_{DD} = (C_d + C_{eq,\pi})V_{DD}\delta(t) + \frac{V_{DD}}{L_{int,tot}\alpha_{d,\pi}}\left(\frac{C_3}{C_2+C_3}\right)^2 e^{-\alpha_\pi t}\sinh\alpha_{d,\pi} t \quad (30)$$

where $\alpha_{d,\pi} = \sqrt{\alpha_\pi^2 - \omega_{p,\pi}^2}$. The total energy delivered by the power-supply for the overdamped transient response is:

$$E_{o,tot}^{xline} = (C_d + C_1 + C_3)V_{DD}^2 - \left(\frac{C_3^2}{C_2+C_3}\right)V_{DD}^2\left(\frac{\omega_{p,\pi}}{\alpha_{d,\pi}}\right)e^{-\frac{\alpha_\pi T}{2}}\sinh\left(\frac{\alpha_{d,\pi}T}{2} + \Psi_\pi\right) \quad (31)$$

We observe that if a CMOS inverter driving a lossy coupled line has an overdamped response, and if $\alpha_\pi - \alpha_{d,\pi} >> 4\pi f_{clock}$, then the energy dissipation per each clock period becomes:

$$E_{o,tot}^{xline} = (C_d + C_{int,tot} + C_L)\, V_{DD}^2 \quad (32)$$

Equations (31) and (32) give the actual and the steady-state energy dissipation per clock period, respectively, when the circuit experiences an overdamped transient response.

In the energy calculations of interconnects driven by CMOS circuits, it was normally assumed that transients in the current and voltage waveforms have been settled to steady state values and the energy was thus simply equal to $(1/2)CV_m^2$. Section 2.a and 2.b showed that this expression can yield quite an inaccurate result for the dissipated energy of the interconnect in high frequency ULSI circuits. Figures 12 and 13 show that modeling a lossy transmission line with a single RLC circuit do not still provide accurate results for the dissipated energy in both underdamped and overdamped cases. These figures show the dissipated energy of a single lossy transmission line for various line lengths when the line is modeled by the RLC-π circuit and compare it with that obtained using a single RLC circuit. For small clock cycles, the RLC circuit model is unable to give a good energy estimate. This is true for both overdamped and underdamped circuits. Figures 12 and 13 also reveal that for both underdamped and overdamped circuits when the clock cycle time is sufficiently long, the results obtained by energy calculations in RLC and RLC-π circuits are both closely equal to $(1/2)CV_m^2$.

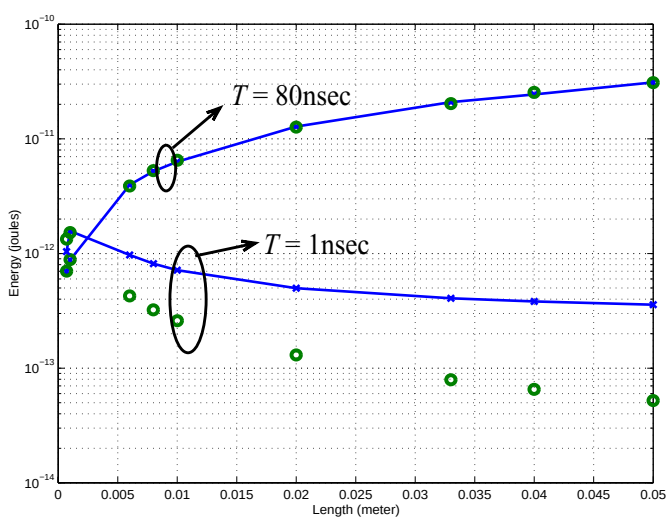

Fig. 12. A comparison between the energy-length variation of the equivalent underdamped RLC-π circuit and that of single underdamped RLC circuit of a lossy transmission line. The comparison has been made for two values of cycle time, T = 1nsec and T = 80nsec

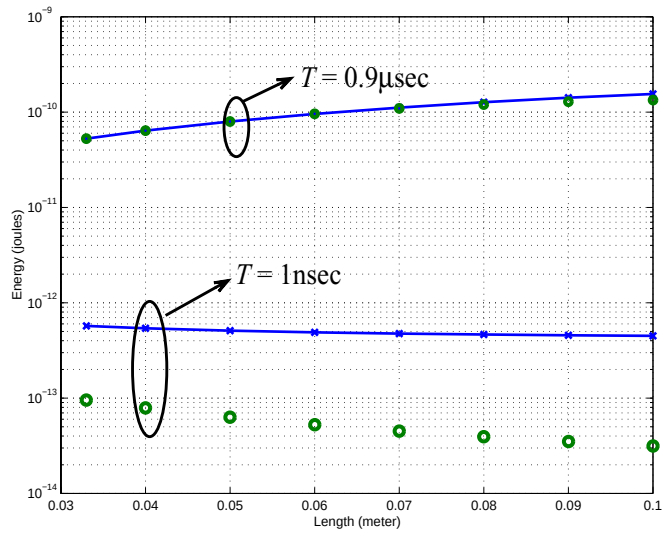

Fig. 13. A comparison between the energy-length variation of the equivalent overdamped RLC-π circuit and that of single overdamped RLC circuit modeling a lossy transmission line. The comparison has been made for two values of cycle time, T = 1nsec and T = 0.9μsec

4. Conclusion and Future Works

This paper presented accurate closed-form expressions for the interconnect energy dissipation in high-speed ULSI circuits. The energy was calculated using an approximate expression for the driving-point impedance of a lossy transmission line. The effect of electromagnetic (inductive and capacitive) couplings on the energy dissipation was also accounted for in the derivations. We synthesize a new stable circuit that is capable of modeling the transmission line for a broad range of frequencies. Several experimental results show that the energy calculated using this circuit is almost equal to the one calculated by directly solving the complicated transmission line equations.

This paper showed that the actual energy dissipation can be quite different from the value predicted by the steady-state $(1/2)CV^2$ model. Using this notion, we will define a new metric that enables us to design interconnects in such a way as to optimize the energy dissipation subject to a given noise margin.

4. References

[1] Semiconductor Industry Associations, International Technology Roadmap for Semiconductors: 2000, http://public.itrs.net/Files/2000UpdateFinal/2kUdFinal.htm.

[2] J. A. Davis, R. Venkatesan, A. Kaloyeros, M. Beylansky, S. J. Souri, K. Banerjee, K. C. Saraswat, A. Rahman, R. Reif, and J. D. Meindl, "Interconnect Limits on Gigascale Integration (GSI) in the 21st Century," *Proceedings of the IEEE*, *Special Issue on Limits of Semiconductor Technology*, Vol. 89, No. 3, pp. 305- 324, March 2001.

[3] T. Uchino, J. Cong, "An Interconnect Energy Model Considering Coupling Effects," *Proceedings of IEEE/ACM Design Automation Conference*, pp. 555-558, Las Vegas, June 2001.

[4] A. Deutsch, P. W. Coteus, G. Kopcsay, H. Smith, C. W. Surovic, B. Krauter, D. Edelstein, P. Restle, "On-chip Wiring Design Challenges for Gigahertz Operation," *Proceedings of the IEEE*, Vol. 89, No. 4, pp. 529- 555, April 2001.